Fully Biogenic Near-Infrared Phosphors: Phycobiliproteins and Cellulose at Force Toward Highly Efficient and Stable Bio-Hybrid Light-Emitting Diodes

Marco Hasler, Marta Patrian, Jesús A. Banda-Vázquez, Sara Ferrara, Andre C. Stiel, JP Fuenzalida-Werner,* and Rubén D. Costa*

Stable/efficient low-energy emitters for photon down-conversion in bio-hybrid light-emitting diodes (Bio-HLEDs) are still challenging, as the archetypal fluorescent protein (FP) mCherry has led to the best deep-red Bio-HLEDs with poor stabilities: 3 h (on-chip)/160 h (remote). Capitalizing on the excellent refolding under temperature/pH/chemical stress, high brightness, and high compatibility with polysaccharides of phycobiliproteins (smURFP), first-class low-energy emitting Bio-HLEDs are achieved. They outperform those with mCherry regardless of using reference polyethylene oxide (on-chip: 24 h vs. 3 h) and new biopolymer hydroxypropyl cellulose (HPC; on-chip: 44 h vs. 3 h) coatings. Fine optimization of smURFP-HPC-coatings leads to stable record devices (on-chip: 2600 h/108 days) compared to champion devices with perylene diimides (on-chip: <700 h) and artificial FPs (on-chip: 35 h). Finally, spectroscopy/computational/thermal assays confirm that device degradation is related to the photo-induced reduction of biliverdin to bilirubin. Overall, this study pinpoints a new family of biogenic emitters toward superior protein-based lighting.

1. Introduction

Over the last decade, inorganic light-emitting diodes (LEDs) have steadily replaced incandescent light bulbs and compact fluorescent lamps.[1] However, they are not considered to be the final solution since i) they contain rare earth and/or toxic

M. Hasler, M. Patrian, J. A. Banda-Vázquez, S. Ferrara,
J.P. Fuenzalida-Werner, R. D. Costa
Technical University of Munich
Chair of Biogenic Functional Materials
Schulgasse, 22, 94315 Straubing, Germany
E-mail: jpf.werner@tum.de; ruben.costa@tum.de
A. C. Stiel
Helmholtz Center Munich
Institute for Biological and Medical Imaging (IBMI)
Ingolstädter Landstraße, 1, 85764 Neuherberg, Germany

The ORCID identification number(s) for the author(s) of this article can be found under https://doi.org/10.1002/adfm.202301820.

materials, ii) they require expensive and harsh production conditions for both, the emitting chips and the inorganic phosphors (IP), and iii) there is a lack of efficient recycling protocols.[2] In other words, materials and processes employed in the fabrication of white-emitting LEDs question the long-term perspective of this technology. In this context, organic LEDs (OLEDs) have been considered as an alternative. Still, they face market entry barriers due to the lack of highly-performing blue-emitting devices and proper recycling protocols, among other problems.[1,3,4]

In this scenario, hybrid LEDs (HLEDs) are quickly evolving with the prospects for replacing IPs by i) organic color down-conversion filters or organic phosphors based on polymer matrices containing small molecules, conjugated polymers, coordination complexes, etc.[5–10] as emitters, ii) perovskite phosphors, in which all-inorganic and metal-halide lead-based perovskites are used,[11] and iii) bio-phosphors.[1,12] The latter are related to an emerging device concept called-Bio-HLED, in which a blue- and/or UV-emitting chip is covered by the bio-phosphor filter that consists of i) a mixture of traditional emitters in biogenic matrices,[13–16] ii) a blend of biogenic emitters (FPs) with conventional polymers,[17,18] or directly in solution,[19] and MOFs,[20] and iii) all-bio color filters, in which both emitters and matrices are biogenic.[21]

FP-based bio-phosphors have shown outstanding development over the last five years.[2,17,18,21,22] The first devices based on FP-polymer photon down-converting coatings showed >100 h of stability with a 10% loss of luminous efficiency (>50 lm W⁻¹) at continuous ambient operating conditions.[2,17] The reduction in luminous efficiency of the FP-polymer coating over time can be explained by the thermally-induced quenching of the fluorophore (FP) caused by protein motion at high photon flux excitation.[22]

Recently, efficient suppression of heat generation was achieved by mastering the mechanical features of the FP-polymer coatings, reaching record efficiencies of ≈130 lm W⁻¹ and stabilities up to 150 days in green-emitting Bio-HLEDs.[18] Besides, FPs were also stabilized in solvent FP-based bio-phosphors, but the device stability was only measured until

**ADVANCED
SCIENCE NEWS**

www.advancedsciencenews.com

**ADVANCED
FUNCTIONAL
MATERIALS**

www.afm-journal.de

100 h.[19] In addition, devices with FP-MOF bio-phosphors were also realized showing maximum efficiencies of 100 lm W^{-1}.[20] Finally, fully biogenic phosphors combining FPs and silk fibroin as packaging matrix were also effective in reducing working temperatures (<40 °C) due to the excellent thermal conductivity of the silk matrix. However, their stability concerning morphological changes over time was critical for the device's performance (i.e., 40 lm W^{-1} stable over 500 h).[21]

All the aforementioned bio-phosphors share the lack of highly emissive and stable deep-red and/or NIR-emitting FPs[23] as a common concern that hinders their application in key areas, such as environmental protection, phototherapy, biosensing, agriculture,[24] night vision technologies,[25] and space communication systems.[26] In this context, mCherry, an FP evolved from DsRed for use in the imaging of mammalian cells,[2,17,27,28] has been the traditional benchmark for red-emitting FPs in lighting devices. Though mCherry features good photostabilities, high expression yields, and good pH tolerance, the emission features are limited by photoluminescence quantum yields (PLQY) of ≈22 % at 610 nm and a molar absorptivity 72000 M^{-1} cm^{-1}, that is, a small brightness coefficient of 15.8.

In this quest for stable and highly emissive deep-red FPs for lighting applications, we present a new design strategy based on proteins of prokaryotic origin. This is motivated by their generally higher stability than that exhibited by their eukaryotic counterparts (i.e., quicker refolding at a much higher temperature, wider pH windows, and higher chemical denaturation tolerance),[29,30] which makes them better suited for the operating conditions of Bio-HLEDs. A prototypical representative of this family is the small Ultra Red Fluorescent Protein (smURFP),[31] a biliverdin binding derivative of a phycobiliprotein that acts as an antenna protein in the photosynthesis process of cyanobacteria. smURFP shows a twofold increased brightness coefficient (i.e., 32.4, molar absorptivity and PLQY values are 180000 M^{-1} cm^{-1} and 18%) and a red-shifted emission spectrum compared to those of mCherry.[31]

Taking inspiration from the polysaccharide-rich environment in which phycobiliproteins typically work,[32] we have introduced a new biogenic HPC matrix. This matrix provides a high density of hydrogen donors and acceptors that can interact with the protein backbone, thus preventing FP motion and photobleaching.[33,34] We demonstrated that the photoluminescent features of smURFP were successfully retained in HPC, leading to fully biogenic NIR-emitting Bio-HLEDs featuring enhanced stabilities compared to those with mCherry (on-chip: 44 h vs. 3 h). In comparison, further optimization of the on-chip configuration led to 2 orders of magnitude enhanced stabilities of ≈2600 h (108 days). This significantly outperforms the prior-art on-chip HLEDs with perylene diimides (≈700 h)[35] and deep-red Bio-HLEDs with artificial FPs (35 h).[36]

Overall, this work sets in three innovative aspects: i) the first establishment of prokaryotic phycobiliproteins as low-energy emitters in lighting devices, outperforming archetypal FPs to date, ii) spectroscopic analysis, computational simulations, and thermal studies to reveal the photo-induced degradation mechanism of smURFP in polymer matrices as stepping stone to better-engineered phycobiliproteins for lighting applications, and iii) the second fully biogenic phosphor using HPC,[37–40]

which is a morphologically and optically much more stable matrix under device operation conditions than those with silk fibroin,[21] leading to record NIR Bio-HLEDs meeting stabilities of 108 days at EQE of 0.82%.

2. Results and Discussion

2.1. Protein Preparation and Characterization

The expression of mCherry and smURFP (**Figure 1**) in bacteria and its further purification were performed following recent protocols reported elsewhere.[41] The absorption spectra of both proteins consist of a well-structured band centered at 587 and 642/390 nm with molar extinction coefficients of 72000 M^{-1} cm^{-1} for mCherry and 180000/60000 M^{-1} cm^{-1} for smURFP (Figure 1) corresponding to their respective chromophores. In addition, both proteins showed the typical absorption band of the aromatic amino acid tryptophan (Trp) centered at 280 nm. The emission spectra show similar well-structured bands peaking at 612/657 and 672/730 nm (Figure 1), respectively. This is associated with similar PLQYs and monoexponential excited-state lifetimes (τ) of ≈20% and 1.9 ns for both proteins (**Table 1**).

2.2. Preparation and Characterization Protein-Polymer Coatings

Following the standard procedure (see Experimental Section),[2,17,22,36] the same amount of proteins (5 nmol) were incorporated in reference non-biogenic polymers that consist of a mixture of trimethylolpropane ethoxylate (TMPE) as a stabilizer and linear poly(ethylene oxide) (PEO) to control the elastomeric features of the final self-standing coatings (**Figure 2**). In the case of the new biogenic HPC matrix, the same amount of both proteins was implemented using the optimized protocol that consists of 3 steps (see Experimental Section): i) dissolve HPC in type I water by gentle stirring, ii) mixing both, HPC and FP solutions, under stirring, and iii) drying following an optimized vacuum protocol. The resulting HPC-protein coatings are stable films that can easily adopt any desired shape (Figure 2).

To the naked eye, the color of the polymer coatings is similar to those of the protein solutions, indicating that the chromophore and its immediate surrounding withstand the coating fabrication (Figure 2). Further confirmation comes from their excitation and emission features. In detail, the excitation and emission spectra of mCherry in TMPE: PEO and HPC coatings are well-structured and slightly blue- and red-shifted compared to those in solution (Figures 1,2; Table 1). This indicates that the interaction of mCherry with the polymers hinders protein agglomeration. However, this might lead to a slightly disrupted tertiary structure, causing a different microenvironment of the chromophore. Indeed, the PLQY increased in TMPE: PEO coatings, while HPC coatings exhibited similar values to those in solution (Table 1). To further investigate the aggregation phenomena,[42,43] the amount of mCherry was 6-fold increased in the polymer coating, showing a broadened excitation spectra shape and a red-shifted emission wavelength
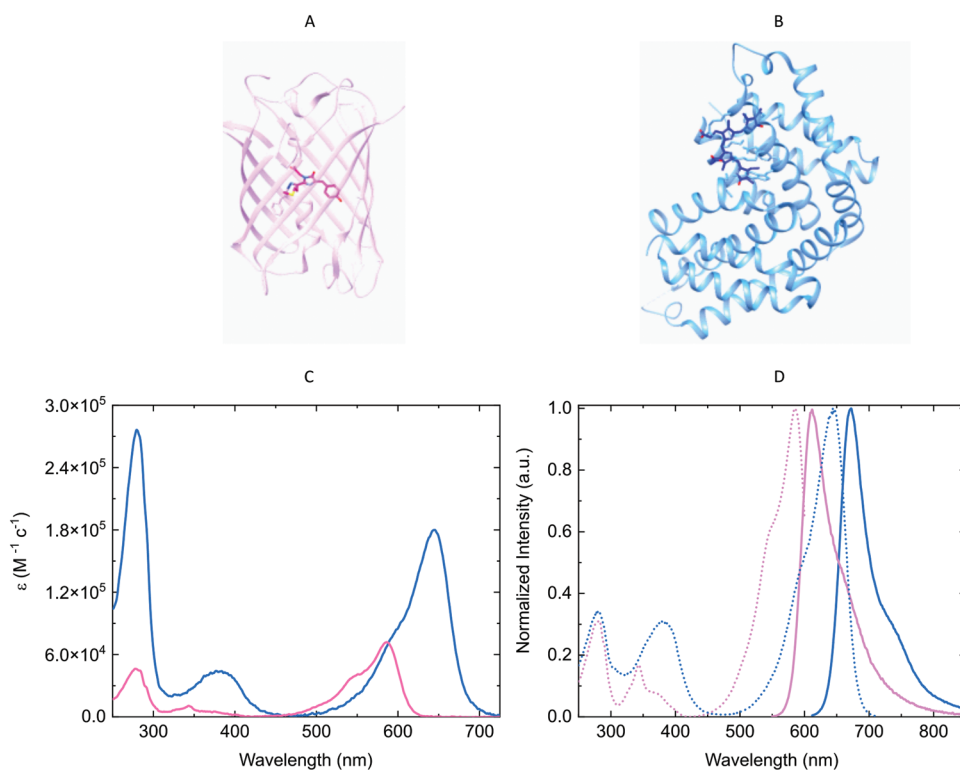
Figure 1. Properties of smURFP and mCherry in solution. Structure of mCherry (A) and smURFP (B), chromophores and directly connected amino acids represented as sticks. Absorption (C) and emission (solid)/excitation (dotted) spectra (D) of mCherry (pink) and smURFP (blue) in PBS buffer solutions.

maxima (≈25 nm) with slightly decreased PLQY and τ values (Figure S1, Table S1, Supporting Information). Therefore, a significant aggregation of the FPs in the coating can be ruled out. Next, the partial disruption of the tertiary structure of the protein structure was analyzed monitoring the emission features of Trp (Figure S2, Supporting Information).[44] These showed a large blue-shifted emission maximum wavelength (≈20 nm) in TMPE: PEO coatings and a reduced τ (0.77 ns) compared to those in solution (1.23 ns). This suggests a more constrained barrel, enhancing the energy transfer process to the chromophore.[45] As such, the protein skeleton is expected to be more distorted, leading to an enhanced PLQY. By contrast, the Trp emission in HPC coatings is slightly red-shifted (≈5 nm) with τ

values of 1.03 ns, indicating that the native protein structure is better retained.

As far as smURFP-polymer coatings are concerned, they showed a similar excitation spectrum with three bands centered at 560, 675, and 390 nm. This strongly contrasts with the spectrum in solution, in which the broadband at 560 nm is not present (Figures 1,2). In line with the excitation features, the emission spectra also consist of a broad emission band with an increased full width at half maximum (FWHM) of 79 and 82 nm and significantly red-shifted maxima to 700 and 719 nm for TMPE: PEO and HPC coatings, respectively. Regardless of the polymer coatings, the PLQY holds constant, while τ slightly changes compared to those in solution (Table 1). In contrast to

Table 1. Photophysical and thermal features of smURFP and mCherry in solution and polymer coatings.

Protein	Matrix	Photophysical characterization								Thermal characterization		
		λ_{exc}[a] [nm]	λ_{max}[b] [nm]	FWHM[c] [nm]	PLQY [%]	τ[d] [ns]	τ[e] [ns]	k_{rad}[f] [s^{-1}]	k_{nr}[g] [s^{-1}]	T_{nr}[h] [°C]	I_{loss}[i] [%]	I_{rec}[j] [%]
mCherry	PBS buffer	586	612	60	21	1.23	1.88	11.2	42.0	64	–	–
	TMPE: PEO	567	606	74	28	0.77	2.11	13.3	34.1	44	33	85
	HPC	587	617	66	21	1.03	1.69	12.4	46.7	40	54	52
smURFP	PBS buffer	644	672	49	17	2.07	2.00	8.5	41.5	37	–	–
	TMPE: PEO	672	700	79	18	1.77	2.45	7.35	33.5	44	35	74
	HPC	672	719	82	16	1.51	1.93	8.3	43.5	87	16	96

[a]Excitation maximum; [b]emission maximum at excitation wavelength λ_{exc}=590 nm; [c]full width at half maximum; [d]λ_{exc} = 280 nm; λ_{em} = 320 nm; short component; [e]λ_{exc} = 280 nm; λ_{em} = λ_{max}; [f]radiative constant; ×10^{-7}; [g]non-radiative constant; ×10^{-7}; [h]non-reversible folding temperature; [i]intensity loss at 50 °C; [j]recovered intensity after heating at 50 °C for 1 h.

**ADVANCED
SCIENCE NEWS**
www.advancedsciencenews.com

**ADVANCED
FUNCTIONAL
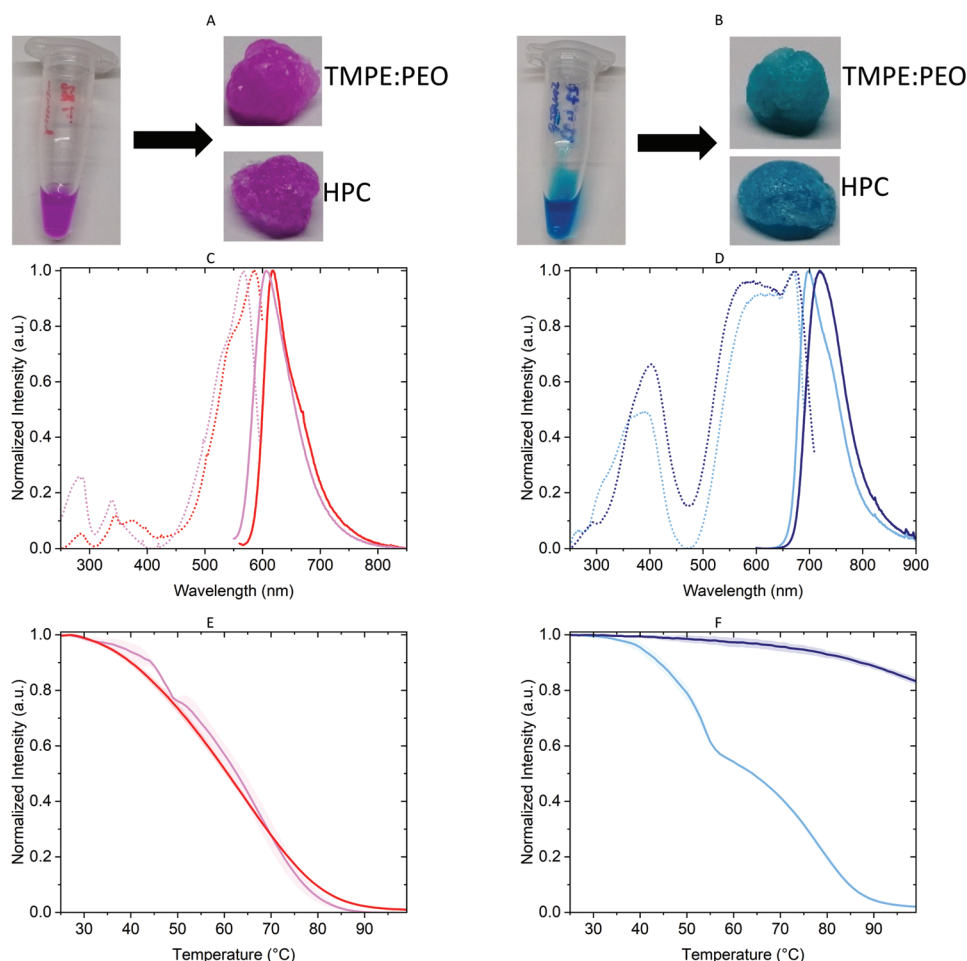MATERIALS**
www.afm-journal.de

Figure 2. Photophysical and thermal properties of polymer coatings. Photographs of mCherry (A) and smURFP (B) PBS buffer solution and polymer coatings. Excitation (dotted line) and emission (solid line) spectra for mCherry (C) and smURFP (D) in TMPE: PEO (light) and HPC (dark) coatings. Modulated scanning fluorometry curves for mCherry (E) and smURFP (F) in TMPE: PEO (light) and HPC (dark) coatings.

archetypal mCherry, these differences point toward a significant aggregation phenomenon. As shown by the X-ray structure (Figure 1),[46] the biliverdin chromophore of smURFP is placed in a partially solvent-exposed cavity created by forming a homodimer of two non-covalently bound proteins. Additionally, smURFP, like every other phycobiliprotein, is prone to form multimeric species in solution.[46,47] Indeed, a 6-fold increase in the protein amount in both coatings led to a slightly broader excitation spectrum. Furthermore, the bands located at ≈390 and 560 nm are more intense, becoming dominant at high protein concentrations. The emission spectra are also red-shifted to ≈735 nm for TMPE: PEO and HPC coatings without affecting the PLQY and τ values upon increasing the protein amount (Figure S1, Table S1, Supporting Information). Thus, aggregation cannot be ruled out in phycobiliprotein-polymer coatings. In addition, the biliverdin chromophore is much more exposed to the solvent environment and exhibits a larger degree of conformational flexibility (i.e., degree of coplanarity, etc.) than the mCherry chromophore.[46,48] Here, water elimination or replacement by the polymer matrices may decrease the polarity of the biliverdin surrounding. At the same time, protein compression upon drying can lead to different biliverdin

conformations, as noted in, for example, the above-mentioned mCherry-polymer coatings. Indeed, the short component for τ of the Trp residue is also reduced in the TMPE: PEO and HPC coatings compared to those in solution (Table 1), indicating that in the distorted protein the Trp to biliverdin distance decreases promoting the energy transfer process. Overall, the complex interplay of the aforementioned factors determines the differences in emission maxima and τ values. All-in-all, smURFP allows the fabrication of photon down-conversion filters with NIR emission maxima (700–750 nm) without affecting PLQY values.

As the next important aspect, we studied the stability of both, TMPE: PEO and HPC self-standing coatings with low amounts of proteins to investigate differences in a shorter timescale. Excellent stability under ambient storage conditions was confirmed for all mCherry polymer coatings as only minor spectroscopic changes (excitation/emission band and PLQY; Figure S3, Supporting Information) over more than one month were noted. While for smURFP, the excitation and emission bands in the TMPE: PEO coating are blue-shifted and less broadened, indicating a slow degradation upon storage. This is also noted by a reduced PLQY. In stark contrast, smURFP
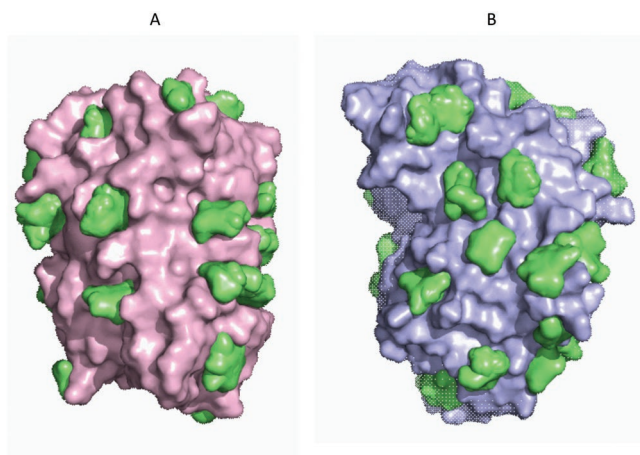
Figure 3. Docking of glucose. Docking of glucose units (green) with mCherry (A) and smURFP (B).

exhibits only slight changes in the HPC coating pointing toward a better stabilization. Furthermore, the temperature-dependent emission upon heating and the thermal stability at 50 °C were studied (Figure S4, Supporting Information; Table 1). Both mCherry-polymer films showed a temperature-induced emission quenching with a loss of emission intensity (I_{loss}) of ≈33% and 45% when reaching 50 °C for the TMPE: PEO and HPC coatings, respectively. In addition, the HPC coatings showed a further linear decrease in emission intensity of ≈10% at 50 °C, suggesting a strong denaturation of the protein over time. Indeed, for TMPE: PEO coatings the emission intensity recovery (I_{rec}) upon cooling reaches 85% of the initial emission intensity, while only 52% is recovered for HPC coatings (Table 1). For smURFP, the TMPE: PEO coatings showed a temperature-dependent emission quenching of ≈30% and a further drop in the emission intensity of ≈5% at 50 °C (Table 1). In stark contrast, the HPC coatings exhibited an emission intensity loss of only 16% and superior thermal stability, with no emission intensity change at 50 °C for 1 h and almost full recovery upon cooling (Table 1). As expected, phycobiliproteins are much more stable in HPC coatings than archetypal mCherry as they have naturally evolved in rich polysaccharide environments.[32] In line with this rationale, computational analysis using the Rosetta suite coupled with Autodock[49,50] (see Experimental Section) revealed that smURFP has more exposed atoms able to interact via hydrogen bonding with cellulose than mCherry (i.e., 147 vs 111; **Figure 3**). Additionally, the Docking of cellulose monomers into all these positions resulted in a total interaction energy of −598.8 and −483.0 Kcal mol^{-1} for smURFP and mCherry, respectively. Thus smURFP is more prone to be stabilized in the HPC matrix than mCherry – vide infra.

To further confirm the thermodynamic stability of the proteins in polymer coatings, we carried out modulated scanning fluorometry assay (Figure 2; Table 1).[51] In line with the above-mentioned findings, mCherry films featured a non-reversible folding temperature (T_{nr}) that strongly reduces from 64 °C in solution (Figure S5, Supporting Information) down to 44 and 40 °C in TMPE: PEO and HPC matrices, respectively (Figure 2; Table 1).[22] A superior stabilization in the TMPE: PEO matrix is expected as it has been optimized to stabilize similar

β-barrel proteins derived from *Aequorea victoria* (i.e., GFP derivatives).[2,17] An opposite behavior is noted for smURFP coatings. On the one hand, the HPC coating showed a stable profile up to 45 °C followed by a slow decrease reaching T_{nr} values 87 °C (Figure 2) that are higher than those in solution (37 °C; Figure S5, Supporting Information), confirming a positive interaction of HPC and smURFP.[52–54] On the other hand, TMPE: PEO coatings showed a gradual decrease reaching T_{nr} values of 44 °C. TMPE is a low molecular weight oligomer and offers a less rigid surrounding than HPC. As a result, it could easily get inside the chromophore cavity of the smURFP, resulting in its irreversible bleaching or quenching. In contrast, HPC offers a more rigid environment with a higher density of hydrogen donors and acceptor groups that can interact with the protein backbone, preventing protein motion and reducing photobleaching,[33,34] as suggested by computational studies. Likewise, polysaccharides have widely led to enhanced stabilities for both, enzymes and proteins,[55] by acting as a crowding agent.[56,57] Furthermore, the addition of sugars, sugar alcohols, and polysaccharides has also improved the thermal stability feature of phycobiliproteins.[58–60] Thus, the combination of smURFP with cellulose derivative matrices is an appealing approach toward fully bio-based phosphors for highly performing HLEDs – vide infra.

2.3. Preparation and Characterization Bio-HLEDs

Bio-HLEDs were prepared by covering a commercial yellow-emitting LED chip (590 nm) with a dome-shaped polymer coating at zero- (on-chip) and 2 cm (remote) distance from the emitting chip (see Experimental Section; **Figure 4**).

To determine the photostability behavior of the protein-polymer coatings, on-chip Bio-HLEDs with both mCherry-polymer coatings with small amounts of protein (5 nmol) were first driven at high applied currents of 200 mA (55 mW cm^{-2}), showing a partial conversion of the LED emission to a well-structured emission band centered at 620/675 (shoulder) nm related to the emission of the FP (Figure 4). Likewise, on-chip Bio-HLEDs with both smURFP-polymer coatings (5 nmol) exhibited a partial conversion toward a broad emission band centered at ≈720 nm (Figure 4). Next, the device stability was studied by monitoring the emission intensity and the temperature of the protein coatings over time. In both mCherry- and smURFP-based on-chip devices, the coating temperature quickly increases up to 30–35 °C for both polymer matrices in similar time scales (Figure 4). Heat generation is related to the non-radiative deactivation of the chromophore and the subsequent heat transfer across the polymer networks depending on the remaining solvent and polymer network morphology.[22] Independent of the type of polymer coatings, the rise of the temperature leads to an initial exponential decrease in the emission intensity for both proteins (Figure 4). In the case of the mCherry devices, this is followed by a rapid exponential reduction of the emission intensity, reaching similar device stabilities of 3 h (i.e., time to get 50% of the initial intensity). In stark contrast, on-chip smURFP-based devices exhibited three processes for both types of polymer coatings: i) an exponential decay related to the rise of temperature, ii) a plateau, and iii) a linear decay (Figure 4). This
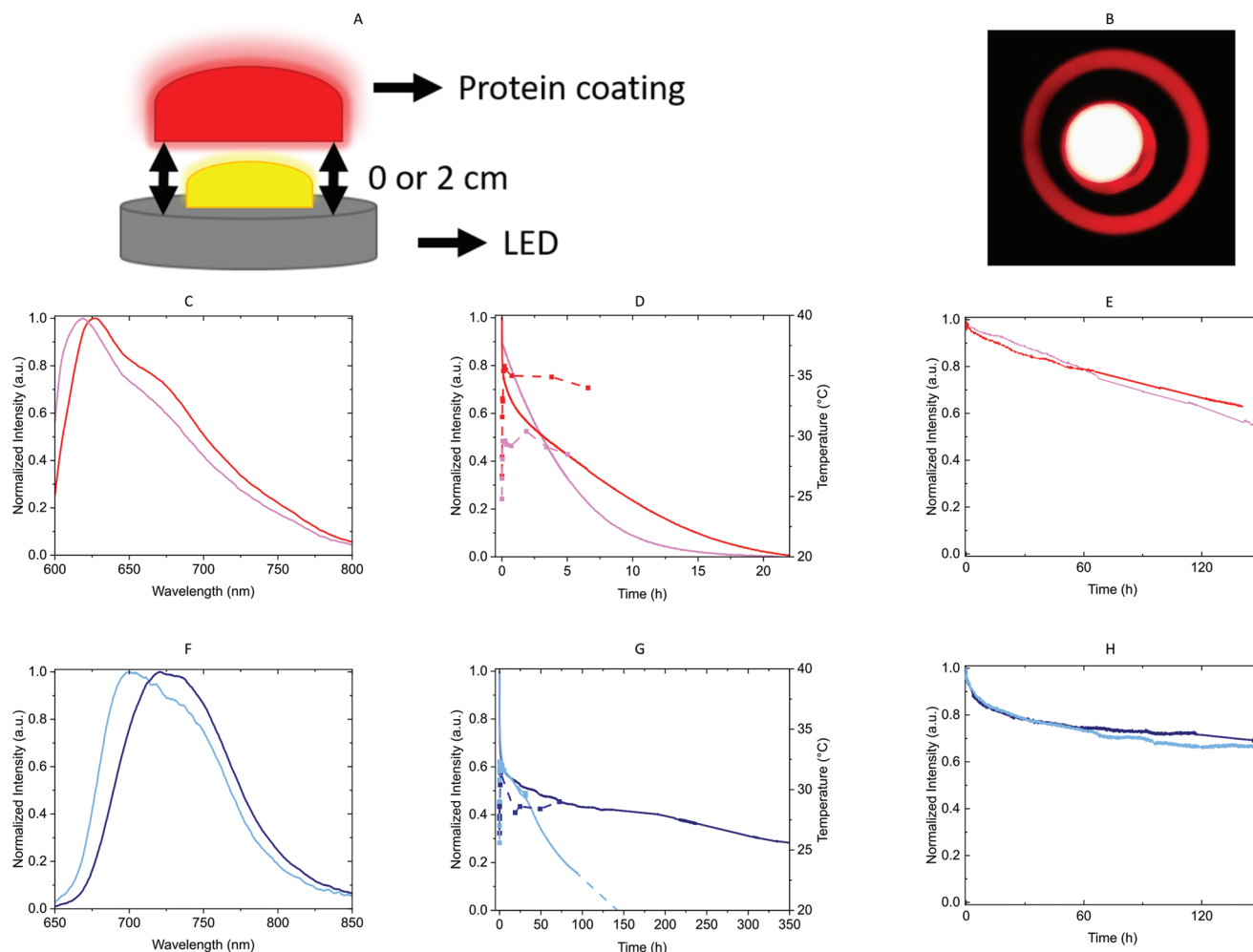
Figure 4. Performance of Bio-HLEDs. Sketch of on-chip and remote HLED architectures (A) and a photograph of the mCherry-HPC-HLED under operation (B) as an example. Emission spectra (C) of the mCherry Bio-HLEDs based on TMPE: PEO (pink) and HPC (red) coatings at 200 mA. Emission intensity decay (solid line) and temperature rise (dashed line) profiles of the mCherry Bio-HLEDs with on-chip (D) and remote (E) configurations based on TMPE: PEO (pink) and HPC (red). Emission spectra (F) of the smURFP Bio-HLEDs based on TMPE: PEO (light-blue) and HPC (dark-blue) coatings at 200 mA. Emission intensity decay (solid line) and temperature rise (dashed line) profiles of the smURFP Bio-HLEDs with on-chip (G) and remote (H) configurations based on TMPE: PEO (light-blue) and HPC (dark-blue).

leads to stabilities (50% initial intensity) of 24 h for TMPE: PEO coatings and 44 h for HPC coatings, that is, an enhancement of one order of magnitude compared to those based on mCherry. The superior performance of smURFP compared to mCherry is attributed to its bilin-like chromophore, which neither shows dark singlet excited states in the range of energies of interest as those reported for mCherry and other structural analogs of eGFP[42,61] nor significant triplet excited states' population.[62] In addition, the difference in stability between polymer coatings is much more significant in smURFP coatings as per mCherry. This is rationalized on the basis of the more favorable interaction/environment that HPC provides for smURFP, enhancing its thermodynamic stability as illustrated by computational studies and the increase in T_{nr} from 44 to 87 °C for TMPE: PEO and HPC coatings, respectively (Table 1).

To further assess the superior photostability of smURFP in polymer matrices with respect to mCherry, remote Bio-HLEDs were studied. Here, the device does not exhibit an increase in temperature upon excitation (Figure 4). In both mCherry-polymer devices, a linear decay of the emission intensity without changing the emission band shape is noted. By contrast, smURFP-based Bio-HLEDs display an initial exponential decrease of the emission intensity over the first 20 h (Figure 4). As above described, smURFP is a homodimer that can feature several conformations with different photostabilities.[41,46,63] Indeed, this has also been described in photostability studies of smURFP in solution, and it has been typically ignored upon comparing photostabilities between proteins.[31] Thus, the first exponential decay is assigned to quick photobleaching of the less photostable oligomers of smURFP. Once this process is over, the emission remains stable for both TMPE: PEO and HPC polymer coatings, showing a small linear decrease related to losses of 35% and 30% over 150 h, respectively. Overall, the device stability using different configurations outperforms those of mCherry devices and is among the best reported to date in the field of hybrid LEDs.[35]
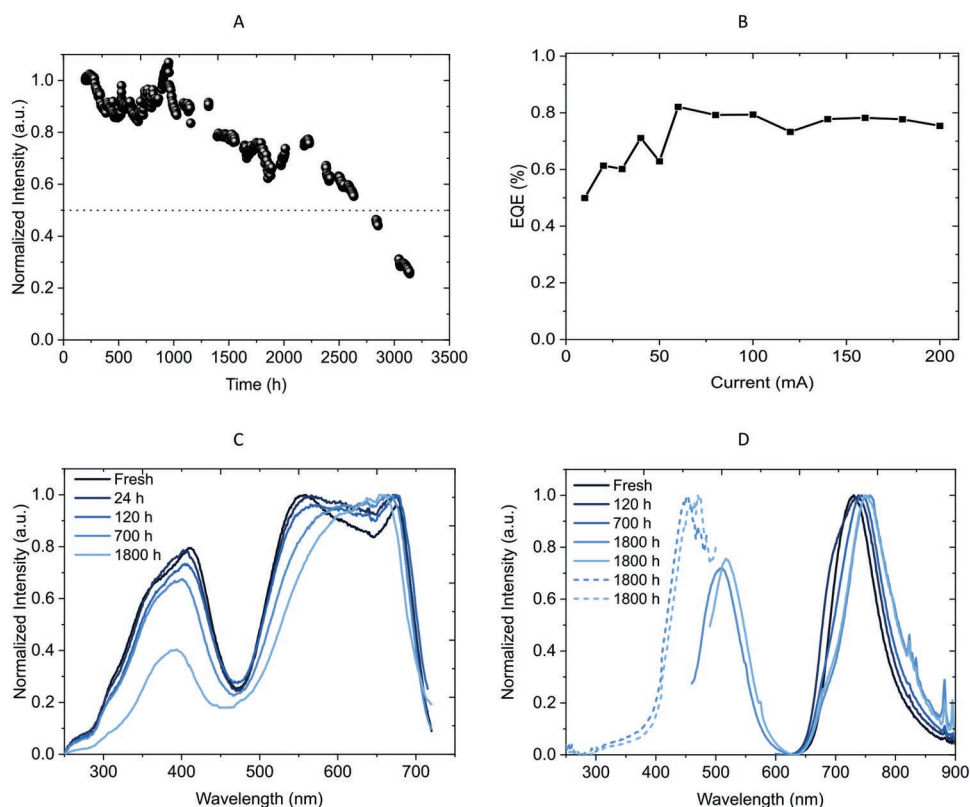
Figure 5. Performance and degradation of smURFP. Emission intensity decay of the smURFP Bio-HLED in on-chip configuration based on HPC (A). EQE values at different driving currents of the smURFP Bio-HLED (B). Excitation spectra of the smURFP Bio-HLED coating over time (C). Emission spectra (solid line) of the smURFP Bio-HLED coating over time and excitation spectra (dashed line) of the newly formed species excited ≈452–470 nm and emitting ≈500–515 nm (D).

To substantiate this statement, we optimized the photon down-conversion features by increasing the amount of smURFP up to 30 nmol and pre-bleaching less stable oligomers in HPC coatings for the on-chip architecture. This allowed us to achieve a total conversion of the LED emission regardless of the applied current, leading to a NIR-HLED with a broad emission band centered at 740 nm that is associated with maximum EQE values of ≈0.82% (**Figure 5**). The stability of the device was monitored at 200 mA (55 mW cm^{-2}), showing a three-stage degradation (Figure 5), that is, a plateau (<15% loss) over 1000 h, followed by a slight linear decrease up to 15% loss for ≈1100 h, and a final quick linear intensity decay of 45% over the following 1000 h. This leads to impressive stability of ≈2600 h or 108 days, which strongly contrasts with the prior-art low-energy bio-HLEDs (on-chip: 30 h).[36]

The device chromaticity holds up to ≈1500 h, when an additional shoulder centered at ≈700 nm starts evolving over time (Figure S6, Supporting Information). Unfortunately, we were unable to study changes in the UV and visible regimes of the coatings in operando devices. This is, indeed, instrumental to understand the photo-induced degradation of smURFP in the HPC matrix. Thus, we coupled this experiment to steady-state/time-resolved emission spectroscopy to monitor changes in the emission/excitation spectra. As shown in Figure 5, the excitation spectra over the first 1200 h changes only slightly, in which a prolonged reduction of the bands centered at 390 and 560 nm

occurs. While the latter suggests that aggregated species are first photo-degraded, the change in the Soret emission intensity indicates that the biliverdin dye is damaged. Indeed, this was confirmed by excitation-dependent emission scans (Figure 5), showing a new emission band after 1800 h, which is centered at 500–515 nm (λ_{exc} = 450–470 nm), and the appearance of a shoulder in the emission band of smURFP at ≈700 nm. The new high-energy emission band is associated with an average $<\tau>$ of 1.78 ns and an excitation spectrum peaking at 452 and 470 nm that is not noted in the excitation spectra of the fresh smURFP-polymer and solution (Figures 1,2 and 5), inferring the lack of an efficient energy transfer process from the degraded species to the smURFP chromophore. This suggests the photo-induced formation of bilirubin via the reduction of the biliverdin chromophore.[64]

3. Conclusion

This work sets in a prokaryotic phycobiliprotein (smURFP) as a new family of low-energy biogenic emitters in Bio-HLEDs, outperforming the stability of state-of-the-art devices using the archetypal mCherry regardless of the type of polymer coatings (i.e., TMPE: PEO: 3 h vs. 24 h; HPC: 3 h vs. 44 h), while fine optimization of fully biogenic photon down-converting coatings based on HPC led to Bio-HLEDs featuring a NIR emission

**ADVANCED
SCIENCE NEWS**

www.advancedsciencenews.com

**ADVANCED
FUNCTIONAL
MATERIALS**

www.afm-journal.de

centered ≈740 nm associated to EQEs of 0.82% and record stabilities of 108 days that represent 2 orders of magnitude jump. This enhancement has been rationalized by combining steady-state and time-resolved spectroscopic/computational/thermal studies. In short, our findings are attributed to the intrinsic photostability of phycobiliproteins that is further enhanced in polysaccharide environments, such as HPC. Finally, spectroscopic assays pointed out that the degradation mechanism of the smURFP devices consists of the formation of bilirubin upon reduction of the native biliverdin chromophore rather than the typical protonation of the chromophore in archetypal FPs.

Overall, this work describes the first integration of phycobiliproteins as emitters in lighting technologies, while we are confident that protein engineering protocols could easily be applied to develop targeted phycobiliproteins for lighting purposes. Here, the investigation of the role and amount of trapped water as well as variants to prevent photon degradation are key aspects. These are ongoing strategies in our labs aiming at enhancing the current devices, which have already overpassed the best performance with respect to low-energy/NIR HLEDs and Bio-HLEDs up to date.

4. Experimental Section

Protein Production: Both proteins, mCherry and smURFP, were expressed in *Escherichia coli* BL21 (DE3) cells in liquid lysogeny broth medium at 30 °C. The cultures were induced with Isopropyl-β-D-1-thiogalactopyranoside at OD_{600} = 0.4 and grown for 24 h at 16 °C. Cells were harvested by centrifugation at 4000 g for 30 min, yielding a pellet that was disrupted with sonication. After centrifugation at 38758 g for 1 h the supernatants were purified using a Ni^{2+} His-Trap column and desalted. A size-exclusion chromatography was carried out for smURFP to separate the dimer. The proteins were flash-frozen in PBS buffer with a 10 mg mL^{-1} concentration and stored at −80 °C. Before use, the proteins were thawed and centrifuged to remove aggregated proteins.

Preparation of Protein Coatings: A mixture of a 4:1 ratio of TMPE: PEO was added to 120 µL of FP solution and stirred under ambient conditions to form a hydrogel. The TMPE: PEO polymer coatings were obtained after a vacuum process from ambient to 15 mbar overnight.[2,22,36] The HPC coatings were prepared as follows. HPC was dissolved in Milli-Q water, type I water, with a concentration of 230 mg mL^{-1} 500 µL of the HPC solution were mixed with 100 µL of FP solution. The final film was obtained after stepwise drying of the solution by vacuum to form a dome-shaped coating. Finally, the coating was dried overnight with a vacuum process going from ambient to 15 mbar.

Experimental Characterization Techniques: Absorption spectra of thawed FP solutions were recorded with a UV–vis-2600i spectrophotometer (Shimadzu) from 250 to 900 nm, with slow scan speed, a data interval of 1 nm, and 1 nm slit width. Photophysical studies were carried out at room temperature using an FS5 spectrofluorometer (Edinburgh Instruments) with a SC-10 module for solid samples, SC-05 for liquid samples, and SC-30 integrating sphere to determine the PLQY. A 280 nm time-correlated single photon-counting module was used to determine τ and adjusted to a monoexponential decay fit with Origin 2021b (OriginLab Corporation, Northampton, MA, USA). The τ of Trp was adjusted to a biexponential decay fit. For the new species formed in smURFP, a 450 nm TCSPC module was used and the average τ was calculated based on the following formula:[65]

$$\langle \tau \rangle = \frac{\sum a_i \tau_i^2}{\sum a_i \tau_i} \tag{1}$$

where a_i are the amplitude fractions and τ_i are the lifetimes. Obtained curves are shown in Figures S7–S9 (Supporting Information). The thermal stability of the FP coatings was measured using the SC-80 module. Coatings were heated from 30 to 50 °C and the temperature was constant for 1 h at 50 °C. Afterward, the coatings were slowly cooled down to 35 °C, and the changes in the emission intensity were monitored.

Modulated Scanning Fluorimetry was performed as previously described in the literature.[51] The Thermocycler CFX96 Touch Real-time PCR System (Bio-Rad) was employed to perform MSF measurements. One program composed of heating and cooling cycles ranging from 25 to 99 °C was used to measure the progressive loss of fluorescence and the irreversible unfolding of the FPs studied in this work. The samples were heated at 5 °C sec^{-1} and held for 1 min at the temperature peak, followed by a recovery period of 5 min at 25 °C. The thermograms were buffer-subtracted and normalized by the highest fluorescence intensity of each sample. Data analysis was performed using Origin 2021b (OriginLab Corporation, Northampton, MA, USA). Mean values and standard deviations of triplicates were calculated and plotted. Modulated scanning fluorometry curves were obtained by plotting the fluorescence values obtained at 25 °C. The nonreversibility temperatures (T_{nr}) were defined as the temperature when 90% of the initial intensity was still recovered upon cooling.

Computational Characterization Techniques: The proteins smURFP (PDB ID 6FZN) and mCherry (PDB ID 2H5Q) were depleted from their heteroatoms with UCSF Chimera 1.16 and relaxed 1000 times with tools with the Rosetta suite,[66] keeping the models with the lowest Total Score for the docking step. For either smURFP or mCherry, the chosen relaxed structure was parameterized with AutoDockTools 1.5.7, as well as the glucose molecule (substance ZINC3833800 at the zinc.docking.org database). The protein structures were scanned for the atoms in their surfaces at a 2.5 Å depth with the FindSurface tool for PyMol 2.3.0. From the surface atoms belonging to side chains of polar or charged amino acids (Arg, Asn, Asp, Cys, Gln, Glu, His, Lys, Pro, Ser, and Thr), the coordinates of N, O or S were used as centers for independent dockings in 20 × 20 × 20 grid boxes. The top solution per docking was kept for estimating the total interaction energy per protein with glucose.

Device Fabrication and Characterization: The dome-shaped phosphors (≈9, 4, and 2 mm for diameter, height, and thickness) were placed either directly on top of the LED (on-chip configuration) or with a distance of 2 cm (remote configuration) and 3–4 replicates were measured for each configuration to exclude external influences. In the remote configuration, a shortpass filter with a cut-off wavelength of 600 nm (Thorlabs) was placed between the LED and the coatings. A 590 nm LED (1 W, WINGER Electronics) was used and driven at 200 mA at ambient conditions. To operate the LED a Keithley 2231A-30-3 was used. Electroluminescence spectra were recorded with an AvaSpec-ULS2048CL-EVO spectrophotometer and an AvaSphere-30 integrating sphere. The temperature was monitored using a thermographic camera ETS320 (FLIR).

Supporting Information

Supporting Information is available from the Wiley Online Library or from the author.

Acknowledgements

Conflict of Interest

The authors declare no conflict of interest.

Data Availability Statement

The data that support the findings of this study are available from the corresponding author upon reasonable request.

Keywords

[1] E. Fresta, V. Fernández-Luna, P. B. Coto, R. D. Costa, *Adv. Funct. Mater.* **2018**, *28*, 1707011.

[2] M. D. Weber, L. Niklaus, M. Pröschel, P. B. Coto, U. Sonnewald, R. D. Costa, *Adv. Mater.* **2015**, *27*, 5493.

[3] S. Reineke, M. Thomschke, B. Lüssem, K. Leo, *Rev. Mod. Phys.* **2013**, *85*, 1245.

[4] D. Volz, M. Wallesch, C. Fléchon, M. Danz, A. Verma, J. M. Navarro, D. M. Zink, S. Bräse, T. Baumann, *GreenChem.* **2015**, *17*, 1988.

[5] I. O. Huyal, U. Koldemir, T. Ozel, H. V. Demir, D. Tuncel, *J. Mater. Chem.* **2008**, *18*, 3568.

[6] G. Heliotis, G. Itskos, R. Murray, M. D. Dawson, I. M. Watson, D. D. C. Bradley, *Adv. Mater.* **2006**, *18*, 334.

[7] E. Gu, H. X. Zhang, H. D. Sun, M. D. Dawson, A. R. Mackintosh, A. J. C. Kuehne, R. A. Pethrick, C. Belton, D. D. C. Bradley, *Appl. Phys. Lett.* **2007**, *90*, 031116.

[8] O. Kim, S. Ha, I. Kim, J. Lee, *ACS Nano* **2010**, *4*, 3397.

[9] C. Ezquerro, E. Fresta, E. Serrano, E. Lalinde, J. García-Martínez, J. R. Berenguer, R. D. Costa, *Mater. Horiz.* **2019**, *6*, 130.

[10] A. A. Wiles, J. Bruckbauer, N. Mohammed, M. Cariello, J. Cameron, N. J. Findlay, E. Taylor-Shaw, D. J. Wallis, R. W. Martin, P. J. Skabara, G. Cooke, *Mater. Chem. Front.* **2020**, *4*, 1006.

[11] Y. Duan, C. Ezquerro, E. Serrano, E. Lalinde, J. García-Martínez, J. R. Berenguer, R. D. Costa, *Adv. Funct. Mater.* **2020**, *30*, 2005401.

[12] V. Fernández-Luna, P. B. Coto, R. D. Costa, *Angew. Chem., Int. Ed.* **2018**, *57*, 8826.

[13] M. S. P. Reddy, C. Park, *Sci. Rep.* **2016**, *6*, 32306.

[14] D. Zhou, H. Zou, M. Liu, K. Zhang, Y. Sheng, J. Cui, H. Zhang, B. Yang, *ACS Appl. Mater. Interfaces* **2015**, *7*, 15830.

[15] H. Tetsuka, A. Nagoya, R. Asahi, *J. Mater. Chem. C* **2015**, *3*, 3536.

[16] K. Benson, A. Ghimire, A. Pattammattel, C. V. Kumar, *Adv. Funct. Mater.* **2017**, *27*, 1702955.

[17] L. Niklaus, S. Tansaz, H. Dakhil, K. T. Weber, M. Pröschel, M. Lang, M. Kostrzewa, P. B. Coto, R. Detsch, U. Sonnewald, A. Wierschem, A. R. Boccaccini, R. D. Costa, *Adv. Funct. Mater.* **2017**, *27*, 1601792.

[18] A. Espasa, M. Lang, C. F. Aguiño, D. Sanchez-deAlcazar, J. P. Fernández-Blázquez, U. Sonnewald, A. L. Cortajarena, P. B. Coto, R. D. Costa, *Nat. Commun.* **2020**, *11*, 879.

[19] S. Sadeghi, R. Melikov, D. Conkar, E. N. Firat-Karalar, S. Nizamoglu, *Adv. Mater. Technol.* **2020**, *5*, 2000061.

[20] X. Wang, Z. Li, W. Ying, D. Chen, P. Li, Z. Deng, X. Peng, *J. Mater. Chem. C* **2020**, *8*, 240.

[21] V. Fernández-Luna, J. P. Fernández-Blázquez, M. A. Monclús, F. J. Rojo, R. Daza, D. Sanchez-deAlcazar, A. L. Cortajarena, R. D. Costa, *Mater. Horiz.* **2020**, *7*, 1790.

[22] V. Fernández-Luna, D. Sánchez-de Alcázar, J. P. Fernández-Blázquez, A. L. Cortajarena, P. B. Coto, R. D. Costa, *Adv. Funct. Mater.* **2019**, *29*, 1904356.

[23] T. J. Lambert, *Nat. Methods* **2019**, *16*, 277.

[24] M. Mao, T. Zhou, H. Zeng, Le Wang, F. Huang, X. Tang, R.-J. Xie, *J. Mater. Chem. C* **2020**, *8*, 1981.

[25] J. Qiao, G. Zhou, Y. Zhou, Q. Zhang, Z. Xia, *Nat. Commun.* **2019**, *10*, 5267.

[26] A. Zampetti, A. Minotto, F. Cacialli, *Adv. Funct. Mater.* **2019**, *29*, 1807623.

[27] U. K. Sukumar, A. Natarajan, T. F. Massoud, R. Paulmurugan, in *Fluorescent Imaging in Medical Chemistry*, 1st ed., (Eds: Z. Cheng), Springer, Cham, Switzerland **2019**, p. 149.

[28] R. N. Day, M. W. Davidson, *Chem. Soc. Rev.* **2009**, *38*, 2887.

[29] W. Colón, J. Church, J. Sen, J. Thibeault, H. Trasatti, K. Xia, *Biochemistry* **2017**, *56*, 6179.

[30] M. Widmann, P. Christen, *J. Biol. Chem.* **2000**, *275*, 18619.

[31] E. A. Rodriguez, G. N. Tran, L. A. Gross, J. L. Crisp, X. Shu, J. Y. Lin, R. Y. Tsien, *Nat. Methods* **2016**, *13*, 763.

[32] C. Bertocchi, L. Navarini, A. Cesàro, M. Anastasio, *Carbohydr. Polym.* **1990**, *12*, 127.

[33] A. M. Bogdanov, A. S. Mishin, I. V. Yampolsky, V. V. Belousov, D. M. Chudakov, F. V. Subach, V. V. Verkhusha, S. Lukyanov, K. A. Lukyanov, *Nat. Chem. Biol.* **2009**, *5*, 459.

[34] H. E. Seward, C. R. Bagshaw, *Chem. Soc. Rev.* **2009**, *38*, 2842.

[35] J. He, S. Yang, K. Zheng, Y. Zhang, J. Song, J. Qu, *Green Chem.* **2018**, *20*, 3557.

[36] S. Ferrara, S. H. Mejias, M. Liutkus, G. Renno, F. Stella, I. Kociolek, J. P. Fuenzalida-Werner, C. Barolo, P. B. Coto, A. L. Cortajarena, R. D. Costa, *Adv. Funct. Mater.* **2022**, *32*, 2111381.

[37] S. P. Hoo, Q. L. Loh, Z. Yue, J. Fu, T. T. Y. Tan, C. Choong, P. P. Y. Chan, *J. Mater. Chem. B* **2013**, *1*, 3107.

[38] F. F. L. Ho, R. R. Kohler, G. A. Ward, *Anal. Chem.* **1972**, *44*, 178.

[39] P. Talik, U. Hubicka, *J. Therm. Anal. Calorim.* **2018**, *132*, 445.

[40] T. G. Rials, W. G. Glasser, *J. Appl. Polym. Sci.* **1988**, *36*, 749.

[41] J. P. Fuenzalida Werner, K. Mishra, Y. Huang, P. Vetschera, S. Glasl, A. Chmyrov, K. Richter, V. Ntziachristos, A. C. Stiel, *ACS Chem. Biol.* **2019**, *14*, 1896.

[42] J. Hendrix, C. Flors, P. Dedecker, J. Hofkens, Y. Engelborghs, *Biophys. J.* **2008**, *94*, 4103.

[43] N. C. Shaner, P. A. Steinbach, R. Y. Tsien, *Nat. Methods* **2005**, *2*, 905.

[44] A. B. T. Ghisaidoobe, S. J. Chung, *Int. J. Mol. Sci.* **2014**, *15*, 22518.

[45] N. V. Visser, J. W. Borst, M. A. Hink, A. van Hoek, A. J. Visser, *Biophys. Chem.* **2005**, *116*, 207.

[46] J. P. Fuenzalida-Werner, R. Janowski, K. Mishra, I. Weidenfeld, D. Niessing, V. Ntziachristos, A. C. Stiel, *J. Struct. Biol.* **2018**, *204*, 519.

[47] H. Scheer, K.-H. Zhao, *Mol. Microbiol.* **2008**, *68*, 263.

[48] P. P. Peng, L. L. Dong, Y. F. Sun, X. L. Zeng, W. L. Ding, H. Scheer, X. Yang, K. H. Zhao, *Acta Cryst.* **2014**, *70*, 2558.

[49] J. K. Leman, B. D. Weitzner, S. M. Lewis, J. Adolf-Bryfogle, N. Alam, R. F. Alford, M. Aprahamian, D. Baker, K. A. Barlow, P. Barth, B. Basanta, B. J. Bender, K. Blacklock, J. Bonet, S. E. Boyken, P. Bradley, C. Bystroff, P. Conway, S. Cooper, B. E. Correia, B. Coventry, R. Das, R. M. De Jong, F. DiMaio, L. Dsilva, R. Dunbrack, A. S. Ford, B. Frenz, D. Y. Fu, C. Geniesse, et al., *Nat. Methods* **2020**, *17*, 665.

[50] O. Trott, A. J. Olson, *J. Comput. Chem.* **2010**, *31*, 455.

[51] H. L. Svilenov, T. Menzen, K. Richter, G. Winter, *Mol. Pharmaceutics* **2020**, *17*, 2638.

[52] D. Matulis, J. K. Kranz, F. R. Salemme, M. J. Todd, *Biochemistry* **2005**, *44*, 5258.

[53] P. Garidel, C. Hoffmann, A. Blume, *Biophys. Chem.* **2009**, *143*, 70.

[54] C. Hoffmann, A. Blume, I. Miller, P. Garidel, *Eur. Biophys. J.* **2009**, *38*, 557.

[55] H. O'Neill, C. V. Angley, I. Hemery, B. R. Evans, S. Dai, J. Woodward, *Biotechnol. Lett.* **2002**, *24*, 783.

[56] S. Shahid, I. Hasan, F. Ahmad, M. I. Hassan, A. Islam, *Biomolecules* **2019**, *9*, 477.

[57] S. B. Jadhav, S. B. Bankar, T. Granström, H. Ojamo, R. S. Singhal, S. A. Survase, *Appl. Microbiol. Biotechnol.* **2014**, *98*, 6307.

[58] I. Chentir, M. Hamdi, S. Li, A. Doumandji, G. Markou, M. Nasri, *Algal Res.* **2018**, *35*, 395.

[59] Y. Huo, X. Hou, Y. Yu, X. Wen, Y. Ding, Y. Li, Z. Wang, *Foods* **2022**, *11*, 1752.

[60] L. Jiang, Y. Wang, F. Zhu, G. Liu, H. Liu, H. Ji, S. Zheng, B. Li, *J. Cancer* **2019**, *10*, 92.

[61] G. Jung, S. Mais, A. Zumbusch, C. Bräuchle, *J. Phys. Chem. A* **2000**, *104*, 873.

[62] R. W. Redmond, J. N. Gamlin, *Photochem. Photobiol.* **1999**, *70*, 391.

[63] J. P. Fuenzalida Werner, Y. Huang, K. Mishra, R. Janowski, P. Vetschera, C. Heichler, A. Chmyrov, C. Neufert, D. Niessing, V. Ntziachristos, A. C. Stiel, *Anal. Chem.* **2020**, *92*, 10717.

[64] D. Chen, J. D. Brown, Y. Kawasaki, J. Bommer, J. Y. Takemoto, *BMC Biotechnol.* **2012**, *12*, 89.

[65] A. Sillen, Y. Engelborghs, *Photochem. Photobiol.* **1998**, *67*, 475.

[66] B. J. Bender, A. Cisneros, A. M. Duran, J. A. Finn, D. Fu, A. D. Lokits, B. K. Mueller, A. K. Sangha, M. F. Sauer, A. M. Sevy, G. Sliwoski, J. H. Sheehan, F. DiMaio, J. Meiler, R. Moretti, *Biochemistry* **2016**, *55*, 4748.

2301820 (10 of 10)